JOURNAL OF MATERIALS SCIENCE 31 (1996) 3289–3297

In situ nuclear magnetic resonance study of defect dynamics during deformation of materials

K. LINGA MURTY
North Carolina State University, Box 7909, Raleigh, NC 27695, USA
K. DETEMPLE, O. KANERT, G. PETERS
University of Dortmund, 44221 Dortmund, FRG
J. TH. M. DeHOSSON
University of Groningen, 9747 AG Groningen, The Netherlands

Nuclear magnetic resonance techniques can be used to monitor *in situ* the dynamical behaviour of point and line defects in materials during deformation. These techniques are non-destructive and non-invasive. We report here the atomic transport, in particular the enhanced diffusion during deformation by evaluating the spin lattice relaxation time in the rotating frame, $T_{1\rho}$, in pure NaCl single crystals as a function of temperature (from ambient to about 900 K) and strain-rate (to $\approx 1.0\,s^{-1}$) *in situ* during deformation. The strain-induced excess vacancy concentration increased with the strain-rate while *in situ* annealing of these excess defects is noted at high temperatures. Contributions due to phonons or paramagnetic impurities dominated at lower temperatures in the undeformed material. During deformation, however, the dislocation contribution became predominant at these low temperatures. The dislocation jump distances were noted to decrease with increase in temperature leading to a reduced contribution to the overall spin relaxation as temperature is increased. Similar tests with an improved pulse sequence (CUT-sequence), performed on ultra-pure NaCl and NaF single crystals revealed slightly different results; however, strain-enhanced vacancy concentrations *were* observed. The applicability of these techniques to metallic systems will be outlined taking thin aluminium foils as an example.

1. Introduction

Many non-destructive experimental techniques have been used to characterize the defects in solids but few of them have been useful in the investigation of the *dynamical* properties of these defects. In particular, there exists a very limited number of techniques that can be used *in situ* in a non-invasive fashion. This is particularly true in the investigation of the diffusion of point defects and motion of dislocations. Nuclear spin resonance methods have been used extensively to investigate the diffusion of point defects in solids at high temperatures, localized motion of atomic defects at low temperatures and the motion of line defects (dislocations) during deformation [1]. At the very beginning of its discovery, nuclear magnetic resonance (NMR) was recognized as one of the most powerful techniques for diffusion studies in materials and has been extensively used to investigate various diffusion parameters such as the activation energies for diffusion in both non-metals and metals [2, 3]. These techniques were extended by Murty and Ruoff [4] to determine the activation volumes for motion and formation of Schottky defect pairs by evaluating the effects of test temperature superimposed by hydrostatic pressure. Because NMR probes the rate of atomic jumps rather directly, one can, in principle, obtain a better microscopic picture of the diffusional process. Later advances, leading to the evaluation of the spin-lattice relaxation times in a rotating frame, resulted in high sensitivity of this parameter to atomic jump processes. Rowland and Fradin [5], Kanert [1] and others were thus able to evaluate the impurity diffusion in alloys. These techniques, in addition, made it possible to probe the jumping dislocations *in situ* during deformation in a non-interactive fashion [6–8]. We have recently reported an investigation of the superimposed effects of deformation on spin-lattice relaxation time (of ^{23}Na) in the rotating frame, $T_{1\rho}$, in single-crystalline pure (≈ 1.5 p.p.m. impurity) NaCl at temperatures from ambient to about 900 K at various constant strain-rates [9] and identified strain-enhanced diffusion at high temperatures and the dislocation contribution at low temperatures. This analysis of strain-enhanced diffusion was based on the vacancy production due to the motion of thermally produced dislocation jogs, while mechanical jogs produced due to the dislocation intersections, could also play a major role [10]. The temperature variation of the flow

0022–2461

stress is needed to detect the dominant type and these data were not available. In addition, the recent modifications of the $T_{1\rho}$ measurements using a novel CUT-sequence method [11] made it possible to follow the signal during the locking time (in the traditional $T_{1\rho}$ technique) which was seen to be of prime significance in the correct evaluation of the free induction decay signal of the deformed material. The traditional $T_{1\rho}$ method assumes no change in the initial magnetization, M_o, of the undeformed versus deformed materials.

We report here the spin relaxation measurements using this CUT-sequence technique on ultra-pure (p.p.b. impurity levels) ^{23}NaCl which made it possible to evaluate the temperature and strain-rate dependencies of the strain-induced vacancy concentration. While these results were slightly different from the earlier data [9], they are in agreement with the models on the strain induced vacancy production [9, 10]. In addition, experiments were performed on NaF^{19} (with no quadrupolar interactions because of spin $I = \frac{1}{2}$) where no dislocation contribution to the spin relaxation is expected. A limited number of tests performed on aluminium thin foils is also presented. These results on the strain-induced vacancy concentration have important bearing on the understanding of the dynamic strain ageing (DSA) and the development of quantitative models characterizing the DSA [12, 13]. In particular, the critical strain, ε_c, for the onset of serrations is related to the strain-induced vacancy concentration and mobile dislocation density [12, 13]

$$\dot{\varepsilon} = A\varepsilon_c^{m+\beta}\exp\left(-\frac{E_m}{kT}\right) \tag{1a}$$

$$C_v^{\varepsilon} \propto \varepsilon_c^{m} \tag{1b}$$

$$\rho_m \propto \varepsilon_c^{\beta} \tag{1c}$$

where C_v^{ε} is the strain-induced vacancy concentration, ρ_m is the density of mobile dislocations and E_m is the activation energy for vacancy migration. These constants $m + \beta$ and E_m are generally evaluated from the strain-rate and the temperature dependencies of the critical strain to serrated flow in tensile tests. The present study enables an evaluation of the strain-induced vacancy concentration rather directly.

2. Strain-induced vacancies

It is well known that plastic deformation results in an increased number of vacancies which are produced from climbing jogs on dislocations [9, 12, 14–20]. While theoretical analyses [14–16] clearly point to the strain-enhanced diffusion due to the excess vacancies produced during plastic deformation, experimental studies (tracer diffusion, creep, etc.) failed to yield consistent results [17–20], and Ruoff and Balluffi [14–16] cited experimental data on creep which exhibited no such presence of excess vacancies. The present NMR study as well as the previous one by Detemple *et al.* [9] clearly revealed the increased vacancy concentration during deformation and made it possible to establish a quantitative relation between the strain-induced vacancy concentration and the applied strain-rate, strain and temperature.

We use the analyses presented elsewhere [9, 10, 12] to derive expressions for the excess vacancy concentration during deformation. It is realized that the excess vacancies produced during deformation migrate to sinks such as the jogs on dislocations and thus these strain-induced vacancies follow the rate equation

$$\dot{C}_v^{\varepsilon} = \dot{C}_v^{\varepsilon}|^{+} + \dot{C}_v^{\varepsilon}|^{-} \tag{2}$$

where the + and − indicate the production and annihilation, respectively. The formation process is governed by the non-conservative motion of jogs on screw dislocations and following Detemple *et al.* [9] we find

$$\dot{C}_v^{\varepsilon}|^{+} = \alpha(T,\varepsilon)\dot{\varepsilon} \tag{3}$$

where α is a strain- (and also perhaps temperature) dependent parameter proportional to the concentration of jogs. If one assumes that the jogs are produced mechanically by dislocation intersections, α will be temperature independent and is proportional to the applied stress and inversely to the jog energy [10] so that the vacancy production rate is given by

$$\dot{C}_v^{\varepsilon}|_{\text{mech}}^{+} = \alpha_1\frac{\sigma}{E_j}\dot{\varepsilon} \quad \text{mechanical jogs} \tag{4a}$$

where α_1 is a constant of the order of 0.1 describing the fraction of the mechanical work used for jog formation, and E_j is the jog formation energy. If, on the other hand, one considers thermally produced jogs [9], we find

$$\dot{C}_v^{\varepsilon}|_{\text{th}}^{+} = \alpha_2\dot{\varepsilon}\exp\left(-\frac{E_j}{kT}\right) \quad \text{thermal jogs} \tag{4b}$$

In both equations, the coefficients α_1 and α_2 are functions of the plastic strain.

At the test temperatures, the strain-produced excess vacancies migrate to appropriate sinks where they annihilate and thus the concentration of these excess vacancies decreases with increased temperatures. In general, dislocations are the primary sinks for the annihilation of the vacancies

$$\dot{C}_v^{\varepsilon}|^{-} = -\beta_0\frac{\Gamma_v}{\lambda^2}C_v^{\varepsilon} \tag{5}$$

where Γ_v is the vacancy jump frequency given by $\Gamma_v = \Gamma_{v0}\exp(-E_m/kT)$ (E_m is the migration energy), β_0 is a coefficient independent of the test conditions, and λ is the sink distance which could be determined either by the strain-dependent dislocation density, ρ ($\lambda^2 \approx 1/\rho$), or by the grain radius, d ($\lambda \approx d$), which is strain independent. The steady state condition, $\dot{C}_v^{\varepsilon} = 0$, leads to the following expressions for the

strain-induced concentration of excess vacancies

$$C_v^{\varepsilon} = \frac{A_i}{\Gamma_v \rho(\varepsilon)} \dot{\varepsilon} \begin{cases} \text{where } A_1 = \alpha_1 \dfrac{\sigma}{\beta_0 E_j} & \text{for mechanical jogs} \\ \text{and } A_2 = \dfrac{\alpha_2}{\beta_0} \exp\left(-\dfrac{E_j}{kT}\right) & \text{for thermal jogs} \end{cases} \tag{6}$$

If the dislocations are the sinks for the vacancies, because $\rho \propto \sigma^2$, we find that

$$C_v^{\varepsilon} \propto \frac{1}{\sigma^i} \exp\left(\frac{E^{(i)}}{kT}\right) \begin{cases} \text{for mechanical jogs, } i = 1,\ E^{(1)} = E_m \text{ and } C_v^{\varepsilon} \propto \sigma^{-1} \\ \text{for thermal jogs, } i = 2,\ E^{(2)} = E_m - E_j \text{ and } C_v^{\varepsilon} \propto \sigma^{-2} \end{cases} \tag{7}$$

so that the total vacancy concentration is given by the sum of those produced thermally and by the divalent impurity and the plastic strain

$$C_v = C_v^{th} + C_v^{++} + C_v^{\varepsilon} \tag{8}$$

where $C_v^{th} = \exp(-E_f/kT)$ with E_f being the vacancy formation energy. For alkali halides (NaCl and NaF), the range of test temperatures falls in the extrinsic region, $C_v^{th} \ll C_v^{++}$.

3. Experimental aspects and results

The materials used were ultra-pure single crystals of NaCl and NaF of size $11 \times 6.5 \times 6.5\,mm^3$ supplied by Dr Korth, Kiel, FRG. The spectrochemical analyses of the samples showed concentrations of divalent impurities (Ca^{2+} and Mg^{2+}) of 12 p.p.b. in NaCl and 100 p.p.b. in NaF, and all these crystals are oriented along the $\langle 0\,0\,1 \rangle$ axis. In addition, pure (99.999%) aluminium foils (25 μm thickness) are also considered.

The nuclear spin relaxation (NSR) rate in the rotating frame, $T_{1\rho}$, was measured as a function of the test temperature while the crystal was deformed along the $\langle 0\,0\,1 \rangle$ direction at a constant strain rate. The experiments were performed in a magnetic field, H_o, of 4.2 T (42 000 G) corresponding to Larmor frequencies of 47.6 MHz for ^{23}Na and 168.2 MHz for ^{19}F by means of a NMR tensile device described in detail elsewhere [9, 11]. In the traditional $T_{1\rho}$ method, a locking pulse, B_1, of far less strength (2–6 G) is applied following a $\pi/2$ pulse for a certain period, t, and the free induction decay at t is recorded (Fig. 1a). The relaxation rate in the rotating frame is then evaluated

$$M_\rho(t) = M_{\rho 0} \exp\left(-\frac{t}{T_{1\rho}}\right) \tag{9}$$

where M is the nuclear magnetization. In the above equation, $M_{\rho 0}$ is the initial magnetization at the beginning ($t = 0$) of the locking field which is often taken to be the signal height, M_0, following the $\pi/2$ pulse, whereas in reality it may be quite different from M_0. In the current CUT-sequence method (Fig. 1b), the locking-pulse is cut into a large number of short pulses with a known separation (time delay $\tau_1 \ll T_2$). If the duration of the short pulses is of the order of $t_p = \pi/4\omega$, we get exactly the relaxation rate in the rotating frame. This technique thus eliminates the uncertainty with regard to the effect of deformation on the initial magnetization, $M_{\rho 0}$, and makes it feasible to obtain the entire magnetization decay signal from the beginning to the end of the locking pulse as shown in Fig. 2a for $^{23}NaCl$ and Fig. 2b for NaF^{19} before and during deformation. The relaxation times derived using this method will be termed $T_{c\rho}$ and are evaluated by fitting the magnetization decay to Equation 9. The number of short pulses was varied from 100–1500 depending on the spin-lattice and spin-spin relaxation times.

Before describing the current experimental data, we present a brief summary of our earlier results on $^{23}NaCl$ [9] and Fig. 3 depicts the temperature variation of the spin-lattice relaxation rate, $1/T_{1\rho}$, obtained using the standard technique (Fig. 1a). The data on undeformed crystals exhibit a phonon contribution at low temperatures, while atomic motion resulted in increased rates at elevated temperature with the maximum corresponding to

$$\tau(T) = \frac{1}{2\omega_{eff}} \tag{10}$$

where $1/\tau$ is the atomic jump frequency and ω_{eff} is the effective Larmor frequency of ^{23}Na nuclei. High-

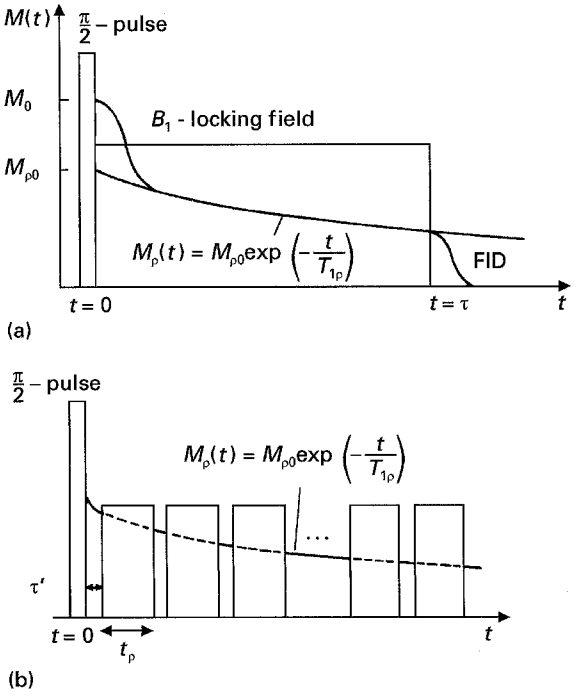

Figure 1 Sequence of pulses used in (a) the traditional $T_{1\rho}$ test method and (b) the current CUT-sequence method, $T_{c\rho}$.

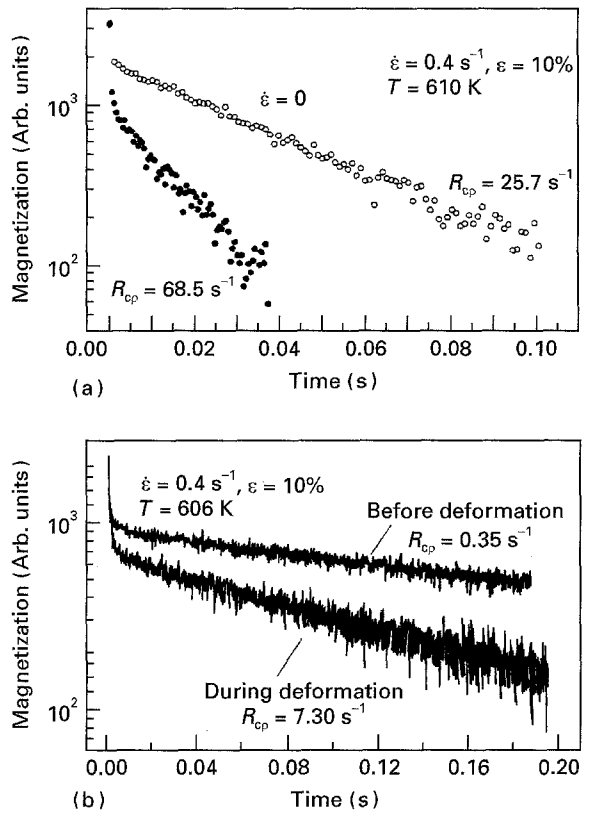

Figure 2 Single-shot measurement of the nuclear magnetization decay $M(t)$ of (a) ^{23}Na in NaCl and (b) ^{19}F in NaF, (○) without and (●) with deformation.

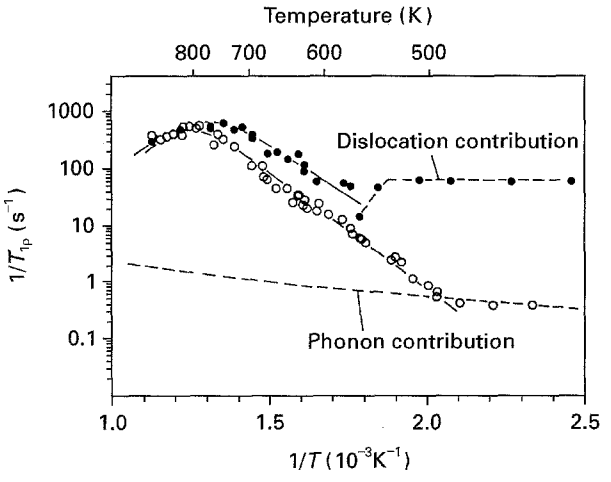

Figure 3 ^{23}Na nuclear spin relaxation rate ($1/T_{1\rho}$) in single crystalline NaCl versus inverse temperature (○) without and (●) (with $\dot{\varepsilon} = 0.4\,s^{-1}$ and $\varepsilon = 15\%$) deformation [9].

temperature data yield the following expression for diffusivity

$$D = D_0 C_v^{++} \exp\left(-\frac{E_m}{kT}\right) \qquad (11)$$

where $D_0 = 3.1\,cm^2\,s^{-1}$, $C_v^{++} = 1.5 \times 10^{-6}$ and $E_m = 0.81$ eV. These values are in good agreement with the literature data on sodium (cation) diffusion in NaCl in the *extrinsic* region where the cation vacancies are produced by Ca^{2+} impurities. Enhanced spin relaxation rates were noted during deformation (at constant strain-rate and strain) as shown in Fig. 3, and these enhancements were shown to arise from the increased vacancy concentration during deformation (Equation 8).

Detemple *et al.* [9] considered thermal jogs on dislocations as the sources for vacancies and obtained the following expression for the strain-induced vacancy concentration, C_v^{ε} from their nuclear spin relaxation rates during deformation

$$C_v^{\varepsilon} = 6.27 \pm 0.14 \times 10^{-7}\,\dot{\varepsilon} \exp\left(+\frac{0.10 \pm 0.03\,eV}{kT}\right) \qquad (12)$$

The decrease in C_v^{ε} at high temperatures is due to *in situ* annealing of strain-induced *excess* vacancies at the appropriate sinks (dislocation jogs).

At low temperatures below about 550 K, dislocation jumps were seen to result in increased spin-lattice relaxation rates [21, 22].

$$\left(\frac{1}{T_{1\rho}}\right)_{\perp} = \frac{\delta_Q \langle V^2 \rangle}{B_1^2 + B_{loc}^2} g_Q(L) \frac{1}{\phi b L} \dot{\varepsilon} \qquad (13)$$

where $(1/T_{1\rho})_{\perp}$ is the relaxation rate due to jumping dislocations obtained by subtracting the phonon contribution from the total relaxation rate at low temperatures, δ_Q is the quadrupolar coupling constant, $\langle V^2 \rangle$ is the mean-squared electric field gradient caused by the dislocations, B_1 is the locking field, B_{loc} is the mean local field in the rotating frame, $g_Q(L)$ is the geometric factor dependent on the dislocation jump distance, L, ϕ is the Schmid factor and $\boldsymbol{b}$ is Burger's vector. As temperature increases, the dislocation jump distance increases, resulting in a reduced effect on the total relaxation rate as noted at temperatures above about 550 K (Fig. 3).

As pointed out earlier, the standard $T_{1\rho}$ method used there assumes that the initial magnetization, M_0, is unaffected by deformation which may not be appropriate, and thus the new improved technique (CUT-sequence) is adopted in the current experiments on NaCl, NaF and aluminium.

3.1. ^{23}Na in NaCl

The spin–spin, T_2, and spin–lattice, T_1, relaxation times were first investigated as a function of the temperature as documented in Fig. 4. The spin–lattice relaxation rates were essentially due to the 2-phonon (Raman) process where $T_1 \propto T^{-2}$. The spin–spin relaxation rate is determined by the *rigid* line width ($1/T_2 \approx \delta\nu_{rigid-lattice}$) at low temperatures which is essentially temperature independent, whereas at high temperatures above about 673 K (400 °C), motional narrowing due to atomic diffusion is reflected as decreased values of T_2 with temperature, the slope of which yields the activation energy for vacancy migration (extrinsic region with athermal divalent impurity-induced vacancy concentration dominating over thermal vacancies). The temperature variation of the spin–lattice relaxation time in the rotating frame, $T_{c\rho}$, determined using the CUT-sequence method is

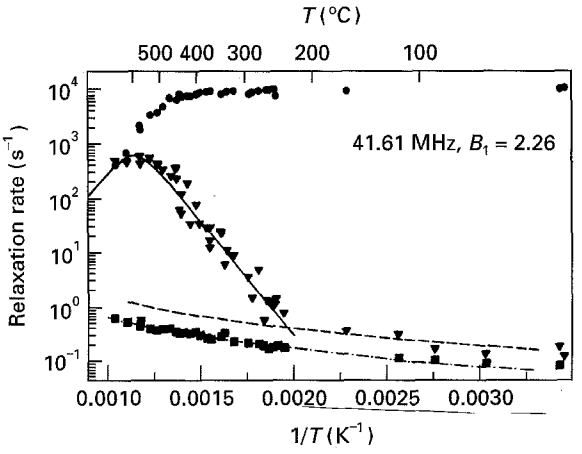

Figure 4 ^{23}Na rates of spin-lattice relaxation ($1/T_1$), spin–spin relaxation ($1/T_2$) and spin–lattice relaxation in the rotating frame from CUT-sequence method ($1/T_{c\rho}$) in NaCl versus inverse temperature. (■) T_1, (▼) $T_{c\rho}$, (●) T_2.

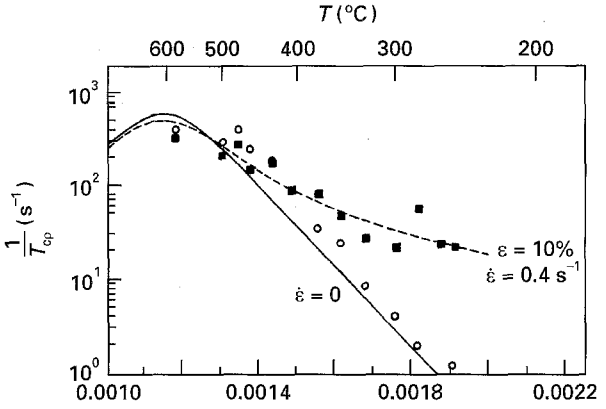

Figure 5 Diffusion-induced part of the spin–lattice relaxation rate in the rotating frame ($1/T_{c\rho}$) versus inverse temperature for ^{23}NaCl (○) without and (■) with deformation. (——, – – –) Model.

also plotted as the rate and we note a dominant effect of atomic motion at high temperatures above about 300 K. The relaxation probability peaked at 873 K as expected from the theoretical calculations of the spectral density, $J(\omega)$, of the motional processes [23] such as in the Torrey and BPP approaches, and also as noted earlier [9]. As is clear from this figure, the relaxation rate in the rotating frame, $1/T_{c\rho}$, is the relevant parameter for investigating the dynamical behaviour of defects.

The temperature variation of the spin–lattice relaxation rate in the rotating frame, $1/T_{c\rho}$, due to atomic motion obtained by subtracting the phonon contribution is depicted in Fig. 5 for both undeformed material and during deformation at a constant strain-rate of $0.4\,s^{-1}$ to 10% strain. We note increased rates of relaxation during deformation especially at lower temperatures. From the maximum in the relaxation rate of the undeformed material, the BPP-curve fit yields the following parameters

$$\langle \omega^2 \rangle = 4.3 \times 10^7\,s^{-2} \tag{14}$$

and

$$\tau_a = 3.98 \times 10^{-10} \exp\left(\frac{0.84\,eV}{kT}\right) s \tag{15}$$

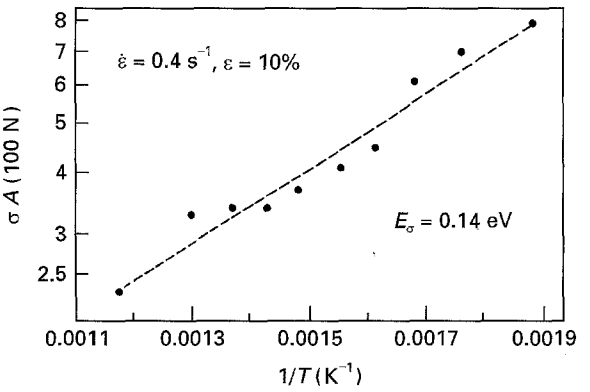

Figure 6 Flow stress, σ, times sample cross-section A, versus inverse temperature in NaCl.

These values compare very well with the earlier data [1, 9] in NaCl. One obtains the diffusion constant with these parameters

$$D = \frac{a_0^2}{6\tau_a} = D_0 C_v \exp\left(-\frac{E_m}{kT}\right)$$

where

$$C_v = C_v^{++} = 12 \times 10^{-9}\,(12\ \text{p.p.b.}) \tag{16}$$

For the deformed material, the strain-induced vacancy concentration adds to the extrinsic vacancies (Equation 8). Assuming that the vacancy jump rate remains unaltered [9], as for the undeformed case, the relaxation rates during deformation can be fitted to the BPP model for the atomic jump times with the total vacancy concentration

$$\frac{1}{T_{c\rho}} = \langle \omega_{sl}^2 \rangle \frac{\tau_a}{1 + 4\omega_{eff}^2 \tau_a^2} \tag{17a}$$

$$\frac{1}{\tau_a} = (C_v^{++} + C_v^{\varepsilon}) \frac{1}{\tau_v} \tag{17b}$$

The line passing through the $T_{c\rho}$ data during deformation (Fig. 5) is obtained from this equation with the following expression for the total vacancy concentration

$$C_v = C_v^{++} + 1.65 \times 10^{-12}\,\dot{\varepsilon} \exp\left(\frac{0.64\,eV}{kT}\right) \tag{18}$$

where the linear strain-rate dependence is used following Detemple *et al.* [9]. Fig. 6 depicts the temperature dependence of the flow stress which yielded an activation energy value of 0.14 eV

$$\sigma = \sigma_0 \exp\left(\frac{E_\sigma}{kT}\right) = \sigma_0 \exp\left(\frac{0.14\,eV}{kT}\right) \tag{19}$$

which is roughly what one expects from the strain-rate equation [20],

$$\dot{\varepsilon} = A\sigma^5 \exp\left(-\frac{0.84\,eV}{kT}\right) \tag{19a}$$

Thus the total vacancy concentration is given by (using Equations 7 and 19)

$$C_v = C_v^{++} + C_\varepsilon^0\,\dot{\varepsilon} \exp\left(\frac{E_v}{kT}\right) \quad \{E_v\}_{expt} = 0.64\,eV \tag{20}$$

where

$$\begin{cases} E_v = E^{(1)} = E_m - E_\sigma = 0.70\,\text{eV} \text{ for mechanical jogs} \\ E_v = E^{(2)} = E_m - E_j - 2E_\sigma \approx 0 \text{ for thermal jogs} \end{cases} \qquad E_\sigma = 0.14\,\text{eV and } E_j = 0.6\,\text{eV}$$

Thus the model based on mechanical jogs predicts a value closer to the experimental measurement and the strain-induced vacancies are thus believed to be produced from athermal jogs created mechanically, as has been proposed by Mecking and Estrin [10] rather than by thermal activation as has been assumed in the earlier analysis [9].

No dislocation contribution is noted in the current data on NaCl during deformation which extend to about 548 K (275 °C). This is not inconsistent with the earlier report [9] which revealed dislocation dominance at temperatures below about 575 K. It will be interesting to extend the present work to lower temperatures to observe this transition.

3.2. ^{19}F in NaF

As pointed out earlier, we wished to examine the ^{19}F nuclear spin relaxation times in NaF especially because only dipolar interactions will be present and thus the dislocations will not have any contribution, albeit the relatively long relaxation times of ^{19}F in NaF make it a rather difficult experiment. As for NaCl, T_1, $T_{c\rho}$ and T_2 are plotted versus inverse temperature for ^{23}NaF (Fig. 7a) and the high-temperature data corresponding to atomic motion were fit to the BPP-model. For NaF^{19}, both the traditional and the CUT-sequence methods (Fig. 1a and b, respectively) were used and the relaxation rates ($1/T_{1\rho}$ and $1/T_{c\rho}$) are plotted versus inverse temperature in Fig. 7b with the temperatures ranging from ambient to about 973 K (700 °C). Although the $T_{c\rho}$ measurements were extended only to about 623 K (350 °C), there is an excellent correlation between the two (for the undeformed material).

The low ($\leqslant 573$ K) temperature data for NaF^{19} reveal decreased relaxation times with temperature which are caused by the dynamics of dilute paramagnetic impurities such as Fe^{3+} or Mn^{2+}. At higher temperatures, the relaxation rate increased due to atomic diffusion. The fit to the BPP-model is performed as in Equation 17 (with subscripts sl for spin–lattice and loc for local)

$$\frac{1}{T_{c\rho}} = \langle\omega_{sl}^2\rangle \frac{\tau_a}{1+4\omega_{eff}^2\tau_a^2} \qquad \begin{cases} \tau_a \propto \exp\left(\dfrac{1.27\,\text{eV}}{kT}\right) \text{ for } ^{23}\text{NaF} \\ \tau_a \propto \exp\left(\dfrac{1.20\,\text{eV}}{kT}\right) \text{ for NaF}^{19} \end{cases} \tag{17a}$$

where $\omega_{eff}^2 = \omega_I^2 + \omega_{loc}^2$ with $\omega_{sl}^2(^{23}\text{NaF}) = 6.1\times10^7\,\text{s}^{-2}$ and $\omega_{sl}^2(\text{NaF}^{19}) = 7.7\times10^9\,\text{s}^{-2}$. It is interesting to note that essentially identical rate equations are obtained from NSR measurements on ^{23}Na and ^{19}F. Various values ranging from 0.45–0.97 eV were reported from experimental investigations of the temperature variation of ^{23}Na spin–lattice relaxation times [24] while the work by Van Steenwinkel [22] on ^{19}F relaxation rates confirmed a value of 0.93 ± 0.13 eV for the cation migration energy in NaF. A much larger value of 1.37 eV was found for the migration energy of anions in NaF [22].

The influence of deformation on the ^{19}F-relaxation rate, $1/T_{c\rho}$, was examined to 623 K (350 °C) at a constant strain-rate of $0.016\,\text{s}^{-1}$ to 10% total strain and enhanced rates were noted (Fig. 7b). Until now, the data were not extended to higher temperatures well into the diffusion region albeit the trend implies no discernible effect. These results are slightly different from those reported earlier (Figs 4 and 5) on NaCl. The relaxation enhancements at low temperatures in the paramagnetic impurity regime cannot be accounted for by the dislocation contribution because we are observing the dipolar interactions and thus it is believed that these enhancements are due to the strain-produced vacancies. The additional contribution to the relaxation rate is given by

$$\left(\frac{1}{T_{c\rho}}\right)_{\text{dynamic}} = \left(\frac{1}{T_{c\rho}}\right)_{\text{total}} - \left(\frac{1}{T_{c\rho}}\right)_{\text{imp}} \tag{21a}$$

where

$$\left(\frac{1}{T_{c\rho}}\right)_{\text{total}} = 0.66\,\text{s}^{-1} \tag{21b}$$

and

$$\left(\frac{1}{T_{c\rho}}\right)_{\text{imp}} = 2.7\times10^{-6}\,T^{1.8} \tag{21c}$$

This implies that the dynamical part of the relaxation rate slightly increases with inverse temperature, and

$$\left(\frac{1}{T_{c\rho}}\right)_{\text{dynamic}} \propto \exp\left(\frac{E^*}{kT}\right) \qquad E^* \approx 0.015\,\text{eV} \tag{22a}$$

and thus one could consider it to be independent of the test temperature. Because the atomic jump frequency is proportional to the dynamical portion of the relaxation rate

$$\Gamma_a = (C_v^{++} + C_v^{\varepsilon})\Gamma_0 \exp\left(-\frac{E_m}{kT}\right) \tag{22b}$$

we expect the following relation to be valid for the strain-induced vacancy dominance (for $\Gamma_a \gg \omega_{eff}$ and

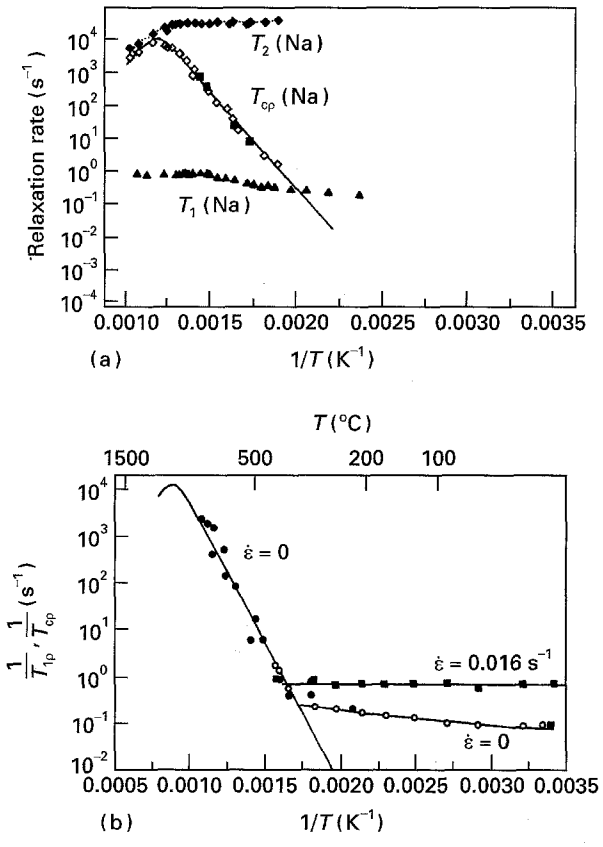

Figure 7 (a) Relaxation rates ((◆) $1/T_2$; (▲) $1/T_1$, (■, ◇), $1/T_{c\rho}$, 4G) for ^{23}Na in NaF versus inverse temperature. (b) Relaxation rates ((●) $1/T_{1\rho}$ and (○, □) $1/T_{c\rho}$; $B_1 = 3.6$ G) for ^{19}F in NaF versus inverse temperature (○) without and (■) with ($\dot{\varepsilon} = 0.016\,s^{-1}$, $\varepsilon = 10\%$) deformation.

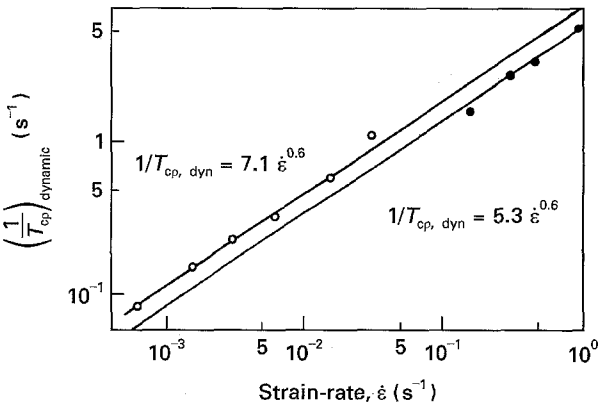

Figure 8 Log–log plot of the strain-rate versus the deformation-induced contribution to the relaxation rate ^{19}F in NaF at (○) 300 and (●) 651 K.

using Equation 7

$$\left(\frac{1}{T_{c\rho}}\right)_{dynamic} = A C_v^{\varepsilon} \Gamma_0 \exp\left(\frac{E_m}{kT}\right) \propto \begin{cases} \exp\left(\dfrac{-E_\sigma}{kT}\right) & \text{for mechanical jogs} \\ \exp\left(\dfrac{E_j - 2E_\sigma}{kT}\right) & \text{for thermal jogs} \end{cases} \tag{22c}$$

In the range of temperatures of interest here, NaF exhibits flow stress which is insensitive to the temperature and $E_\sigma \approx 0$ while $E_j \approx 0.6$ eV [9]. Thus the model based on the thermal jogs predicts a value of E^* (Equation 22a) which is more than an order of magnitude higher than the experimental value. The Mecking–Estrin mechanical jog model [9], on the other hand, accurately predicts the current experimental finding of the temperature insensitive $(T_{c\rho})_{dynamic}$ similar to NaCl.

As before, the strain-rate dependence was examined in NaF also; however, a deviation from the linear dependence was noted as shown in Fig. 8 where the dynamical part of the relaxation rate is plotted versus the applied strain-rate on a double-log plot at 300 and 651 K

$$\left(\frac{1}{T_{c\rho}}\right)_{dynamic} \propto (\dot{\varepsilon})^{0.6} \tag{22d}$$

The lower sensitivity to the applied strain-rate may be due to the strain-rate (or flow stress) dependence of the sink distance and for the dominance of mechanical jogs [10], the strain-induced vacancy concentration is proportional to the square of the sink distance

$$C_v^{\varepsilon} \propto \lambda^2 \sigma\dot{\varepsilon} \propto \frac{\sigma\dot{\varepsilon}}{\rho}$$

$$\propto \frac{\dot{\varepsilon}}{\sigma} \propto \dot{\varepsilon}^{1-m} \tag{22e}$$

for dislocations being the vacancy sinks. With $m \approx 0.2$, we find that the strain-rate exponent in the Equation 22d should be about 0.8; however, such deviation from unity is not noted in NaCl.

3.3. ^{27}Al in metallic aluminium

Aluminium was chosen because thermal vacancies are dominant in metals and also DSA has been extensively investigated in aluminium based alloys [13]. Moreover, the aluminium nucleus is amenable for NSR measurements. Unfortunately, the problem with the skin-effect in metallic systems limits the study to thin foils which makes it relatively more difficult to perform deformation-NMR experiments. We present here some preliminary results obtained to-date while the experimental details will be published elsewhere. The nuclear spin relaxation rates were determined on thin (25 μm) foils of 99.999% pure aluminium tensile specimens (grain size ≈ 150 μm) of about 10 mm wide and 27 mm gauge length. Relatively short relaxation times (~ 5 ms) created some unexpected problems in the relaxation experiments during deformation.

As for NaCl, the temperature variations of the spin–spin ($1/T_2$) and spin–lattice ($1/T_1$ and $1/T_{c\rho}$)

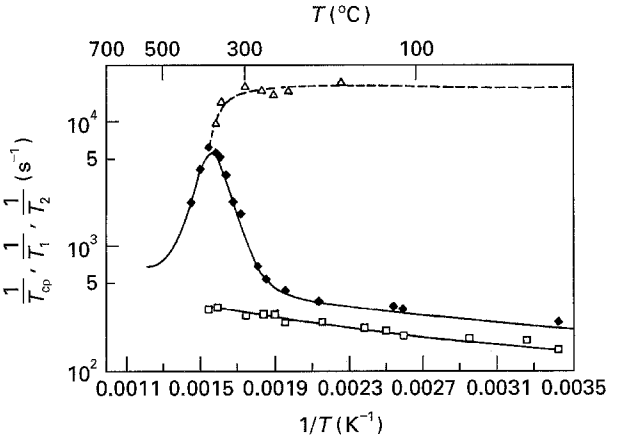

Figure 9 ^{27}Al rates of spin–lattice relaxation ((□) $1/T_1$), spin–spin relaxation ((△) $1/T_2$) and spin–lattice relaxation in the rotating frame using CUT-sequence method ((◆) $1/T_{c\rho}$), $B_1 = 2.4$ G) in 99.999% pure aluminium versus inverse temperature.

relaxation rates of ^{27}Al are shown in Fig. 9. Below about 473 K (200 °C), the spin–lattice relaxation rates are caused by conduction electrons (Korringa relaxation process: $1/T_1 \propto T$) while $1/T_2$ is given by the *rigid* line width analogous to NaCl. However, at higher temperatures, $1/T_2$ decreases due to the motional narrowing of the line width, and $1/T_{c\rho}$ exhibited a dramatic increase with the characteristic peak (diffusion-induced relaxation processes [1, 2]) as for NaCl and NaF. Again, T_1 failed to demonstrate this relaxation contribution. The motional part of $1/T_{c\rho}$ is fitted to the BPP expression as before (modified for the field-dependence)

$$\frac{1}{T_{c\rho}} = \frac{\omega_1^2 + \delta\omega_{loc}^2}{\omega_1^2 + \omega_{loc}^2}\left(\langle\omega_{sl}^2\rangle \frac{\tau}{1 + 4\omega_{eff}^2\tau^2}\right) \quad (23b)$$

from which the atomic jump rate is obtained as

$$\frac{1}{\tau} = \Gamma_a = \Gamma_{a0}\exp\left(-\frac{E_m + E_f}{kT}\right) = 5 \times 10^{14}\exp\left(-\frac{1.27\,\text{eV}}{kT}\right)\text{s}^{-1} \quad (23c)$$

These values for the pre-exponential factor and activation energy are in excellent agreement with earlier data on aluminium [25] including the activation energies for self-diffusion and high-temperature creep [26].

The effect of deformation on the relaxation rate was also observed. Fig. 10a depicts the time variation of the applied strain and the resulting flow stress while the corresponding relaxation rate ($1/T_{c\rho}$) is shown in Fig. 10b which clearly demonstrates the enhancement of the rate during deformation. It is interesting to note the drop in the spin relaxation rate during load relaxation (at constant load, Fig. 10a) though the rate remains larger than that for the undeformed material.

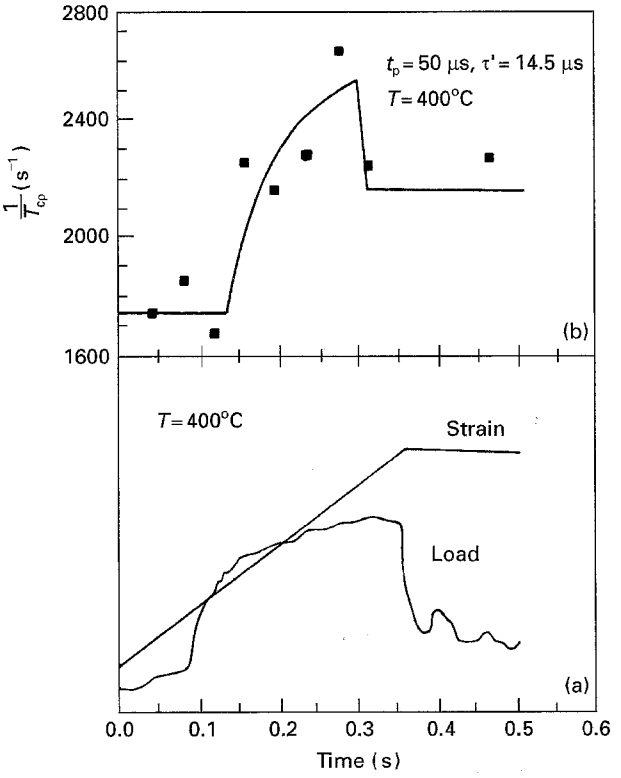

Figure 10 Time variation of (a) load and strain, and (b) the corresponding ^{27}Al relaxation rate in the rotating frame using the CUT-sequence, $1/T_{c\rho}$ in 99.999% pure aluminium at 670 K. Note the enhancement of the relaxation rate under applied load (b).

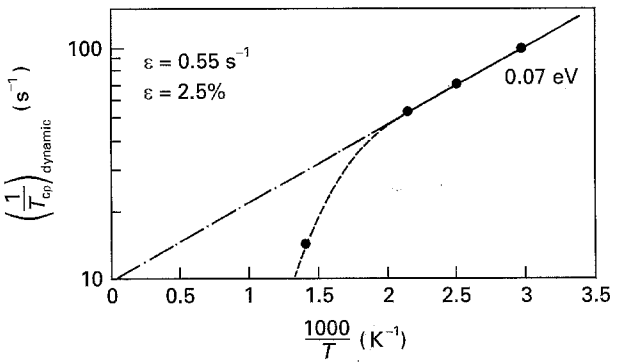

Figure 11 Deformation-induced part of ^{27}Al spin–lattice relaxation rate in the rotating frame, $1/T_{c\rho}|_{dynamic}$, versus inverse temperature in 99.999% pure aluminium.

Further, first preliminary experiments were performed on the temperature variation of the strain-induced contribution to the relaxation rate ($1/T_{c\rho}|_{dynamic}$), and the results are shown in Fig. 11. Obviously, the relaxation rate increases weakly with decreasing temperature below about 500 K dropping off sharply at elevated temperatures. The small value of the slope of about 0.07 eV observed at low temperatures seem to favour the model of mechanically formed jogs [10]. Then, according to Equation 22c, the relaxation rate becomes nearly temperature independent as for NaF. Further NMR experiments on aluminium under deformation are in progress, and the results will be presented in the future.

Acknowledgements

The work is based on a paper presented at the TMS Fall Meeting, Pittsburgh, PA, October 1993, and was supported by the Deutsche Forschungsgemeinschaft and the Foundation for Fundamental Research on Matter (FOM). We acknowledge the travel grants provided by the Government of Nordrhein-Westfalen and North Carolina Board of Science and Technology.

References

1. O. KANERT, *Phys. Rep.* **91** (1982) 183.
2. N. BLOEMBERGEN, E. M. PURCELL and R. V. POUND, *Phys. Rev.* **73** (1948) 679.
3. C. P. SLICHTER, "Principles of Magnetic Resonance" (Springer, Berlin, 1990).
4. K. L. MURTY and A. L. RUOFF, *Phys. Rev.* **B1** (1970) 114.
5. T. J. ROWLAND and F. Y. FRADIN, *ibid.* **182** (1969) 760.
6. H. J. HACKELOER, O. KANERT, H. TAMLER and J. Th. DE HOSSON, *Rev. Sci. Instrum.* **54** (1983) 341.
7. W. H. M. ALSEM, J. TH. DE HOSSON, H. TAMLER and O. KANERT, *Philos. Mag.* **46** (1982) 451.
8. K. L. MURTY and O. KANERT, *J. Appl. Phys.* **67** (1990) 2866.
9. K. DETEMPLE, O. KANERT, K. L. MURTY and J. Th. DE HOSSON, *Phys. Rev.* **B44** (1991) 1988.
10. H. MECKING and Y. ESTRIN, *Scripta Metall.* **14** (1980) 815.
11. G. PETERS, Diplomat Thesis, University of Dortmund (1993).
12. K. L. MURTY, F. A. MOHAMED and J. E. DORN, *Scripta Metall.* **5** (1971) 1087.
13. P. G. McCORMICK, *Acta Metall.* **36** (1988) 3061.
14. A. L. RUOFF and R. W. BALLUFFI, *J. Appl. Phys.* **34** (1963) 1848.
15. *Idem. ibid.* **34** (1963) 2862.
16. A. L. RUOFF, *ibid.* **38** (1967) 3999.
17. K. HIRANO, M. COHEN, B. L. AVERBACH and N. UJIYE, *Trans. AIME* **227** (1963) 950.
18. A. R. WAZZAN and J. E. DORN, *J. Appl. Phys.* **36** (1965) 222.
19. C. H. LEE and R. MADDIN, *Trans. AIME* **215** (1959) 397.
20. K. LINGA MURTY, *Mater. Sci. Eng.* **14** (1974) 217.
21. K. LINGA MURTY, D.BEGERT, R. MUNTER and O. KANERT, *J. Am. Ceram. Soc.* **73** (1990) 861.
22. R. VAN STEENWINKEL, *Z. Naturforsch.* **29** (1974) 278.
23. D. WOLF, *Spin-Temperature and Nuclear-Spin Relaxation in Matter* (Clarendon, Oxford, 1979).
24. K. LINGA MURTY, *Scripta Metall.* **3** (1969) 939.
25. F. Y. FRADIN and T. J. ROWLAND, *Appl. Phys. Lett.* **11** (1967) 207.
26. J. E. BIRD, A. K. MUKHERJEE and J. E. DORN, in "Quantitative Relations Between Properties and Microstructure", edited by D. G. Brandon and A. Rosen (Israel University Press, 1969).

Received 6 September 1994
and accepted 1 December 1995